Research Square

Preprints are preliminary reports that have not undergone peer review.
They should not be considered conclusive, used to inform clinical practice,
or referenced by the media as validated information.

Parthenolide enhances imatinib activity in gastrointestinal stromal tumor models through stress-associated apoptosis

Longyi Piao
Yanbian University
Zheng-Gen Piao
Yanbian University Hospital
Chun-Hua Zheng
University of Health and Rehabilitation Sciences
Dongyuan Xu
Yanbian University
Xi-Hui Li
Yanbian University Hospital
Pengcheng Wei
Yanbian University Hospital
Cho Park
Yanbian University Hospital
Chuang-Ming Zheng
Yanbian University
Toufeng Jin
tfjin@ybu.edu.cn

Yanbian University Hospital

Research Article

Keywords: Gastrointestinal stromal tumor, parthenolide, imatinib, drug sensitization, apoptosis, endoplasmic reticulum stress

Posted Date: July 13th, 2026

DOI: https://doi.org/10.21203/rs.3.rs-10231293/v1

License: This work is licensed under a Creative Commons Attribution 4.0 International License.
Read Full License

Additional Declarations: No competing interests reported.

Version of Record: A version of this preprint was published at Investigational New Drugs on September 15th, 2026. See the published version at https://doi.org/10.1007/s10637-026-01631-1.

Abstract

Purpose

Imatinib remains a key treatment for gastrointestinal stromal tumors (GISTs), but incomplete response and acquired resistance limit durable disease control. This study evaluated whether parthenolide (PTL) enhances imatinib activity in GIST models and explored associated stress-response mechanisms.

Methods

Public GIST transcriptomic datasets were analyzed to identify cell-fate and stress-related programs associated with imatinib response. GIST-T1 and GIST-882 cells were treated with PTL, imatinib, or PTL plus imatinib. Cell viability, migration, colony formation, apoptosis, reactive oxygen species (ROS), mitochondrial membrane potential, ultrastructure, ER-stress markers, and autophagy-associated proteins were examined. A GIST-T1 xenograft model was used for in vivo validation.

Results

Transcriptomic analyses suggested that imatinib response was associated with apoptosis-, stress-, and survival-related programs. PTL and imatinib inhibited GIST cell growth in a dose-dependent manner, and PTL plus imatinib produced stronger suppression of migration and colony formation than either monotherapy. The combination increased apoptotic cell death, elevated ROS, disrupted mitochondrial membrane potential, induced mitochondrial structural injury, increased p-IRE1α/IRE1α and CHOP, and altered LC3B, Beclin-1, and PINK1 expression. In xenografts, PTL plus imatinib produced the lowest endpoint tumor weights and significantly reduced tumor weight compared with vehicle control, without greater body-weight loss than imatinib alone.

Conclusion

PTL enhanced the antitumor activity of imatinib in GIST models. These findings support further investigation of PTL-based imatinib-sensitization strategies.

Introduction

Gastrointestinal stromal tumors (GISTs) are molecularly defined mesenchymal tumors, most commonly driven by activating alterations in KIT or PDGFRA [1]. This biology has made GIST one of the clearest examples of targeted therapy in solid tumors. Imatinib, a KIT/PDGFRA inhibitor, remains the standard first-line systemic treatment for advanced or unresectable GIST with imatinib-sensitive genotypes [1, 2]. Its introduction changed the treatment of GIST, but the benefit is often not permanent.

Acquired resistance remains a major barrier to long-term disease control. Resistant disease frequently emerges through secondary kinase-domain mutations, polyclonal tumor evolution, reactivation of downstream survival signaling, and non-KIT/PDGFRA-dependent adaptive mechanisms [3, 4]. Later-line tyrosine kinase inhibitors (TKIs), including ripretinib and avapritinib in selected molecular settings, have improved the treatment landscape [5, 6]. However, sequential kinase inhibition does not fully solve disease persistence. This provides a rationale for pharmacological strategies that may deepen or prolong the response to imatinib.

One such strategy is to interfere with the stress-handling capacity of GIST cells. Tumor cells exposed to targeted therapy may survive by engaging mitochondrial regulation, unfolded protein response signaling, autophagy, and anti-apoptotic programs. In GIST models, imatinib-induced autophagy has been reported as a survival response, and autophagy inhibition can promote cell death during imatinib treatment [7]. This suggests that stress-response pathways may influence whether imatinib-treated cells remain viable or shift toward apoptosis.

Parthenolide (PTL), a sesquiterpene lactone derived from feverfew, has been studied as a bioactive compound with anticancer and chemosensitizing potential. PTL has been reported to modulate pro-survival signaling, induce apoptosis, and cooperate with established anticancer agents in several tumor models [8]. Notably, PTL activity has also been linked to oxidative stress, mitochondrial injury, and apoptosis-associated signaling, although the dominant mechanism may vary by cellular context [9, 10]. These properties make PTL a plausible candidate for combination treatment in settings where tumor cells rely on adaptive stress responses after targeted therapy.

Whether PTL enhances imatinib activity in GIST has not been systematically tested in paired GIST models. In this study, public transcriptomic datasets were analyzed as hypothesis-generating resources to identify stress- and cell-fate-related programs associated with imatinib response. We then examined PTL, imatinib, and PTL plus imatinib in GIST-T1 and GIST-882 cells, followed by xenograft validation. This study aimed to provide preclinical evidence for PTL-based enhancement of imatinib activity.

Materials and methods

Cell lines, reagents and culture conditions

Human GIST-T1 cells were obtained from Fenghbio Co., Ltd. (cat. no. SC01830239; Changsha, Hunan, China), and human GIST-882 cells were obtained from Shanghai Enzyme-linked Biotechnology Co., Ltd. (cat. no. ml096125; Shanghai, China). Cells were cultured in Dulbecco's modified Eagle's medium with 10% fetal bovine serum and 1% penicillin–streptomycin at 37°C and 5% CO2 and used during logarithmic growth.

Cell-line identity was authenticated by STR profiling performed by the suppliers before shipment. Before use, both cell lines were tested for mycoplasma contamination using the BeyoColor™ Mycoplasma Red

and Yellow Colorimetric LAMP Assay Kit with UDG (cat. no. C0307S; Beyotime Biotechnology, Shanghai, China). Both cell lines tested negative.

PTL and imatinib were purchased from Shanghai YuanYe Bio-Technology Co., Ltd. (Shanghai, China). Stock solutions were prepared in dimethyl sulfoxide and freshly diluted in culture medium before use. Final dimethyl sulfoxide concentration was kept at ≤ 0.1%.

Cell viability, dose selection and functional assays

Cell viability was measured using the MTT assay. GIST-T1 and GIST-882 cells were seeded into 96-well plates at 2 × 10^3 cells/well and allowed to adhere for 24 h. For time-course experiments, cells were treated with PTL or imatinib for 24, 48, or 72 h. GIST-T1 cells were treated with 5, 10, 15, and 20 μM PTL, whereas GIST-882 cells were treated with 5, 10, 20, and 40 μM PTL. For imatinib treatment, both cell lines were treated with 0.02, 0.05, 0.10, and 0.20 μM imatinib.

For 48-h dose–response analysis, PTL was tested at 0–40 μM, and imatinib was tested at 0–0.50 μM. After treatment, 10 μL of MTT solution (5 mg/mL; Beijing Baiao Laibo Technology Co., Ltd.; Beijing, China) was added to each well and incubated for 3 h at 37°C. Formazan crystals were dissolved in 150 μL DMSO, absorbance was measured at 492 nm using a Multiskan FC microplate reader (Thermo Fisher Scientific Inc.), and growth inhibition was calculated relative to vehicle control. IC50 values were estimated from 48-h inhibition curves using a four-parameter logistic regression model in OriginPro 2024b (OriginLab Corporation, Northampton, MA, USA). Cell-line-specific working concentrations close to the estimated IC50 values were used for subsequent assays: 20 μM PTL and 0.10 μM imatinib for GIST-T1 cells, and 27 μM PTL and 0.30 μM imatinib for GIST-882 cells.

For wound-healing assays, cells were seeded in 6-well plates, grown to > 90% confluence, scratched with a sterile 10-μL pipette tip, and cultured in serum-reduced medium containing vehicle, PTL, imatinib, or PTL plus imatinib. Images were captured at 0 and 48 h and analyzed using ImageJ. For colony-formation assays, cells were seeded at 600–800 cells/well in 6-well plates, treated for 10–14 days, fixed, stained with crystal violet, and colonies containing at least 50 cells were counted.

Apoptosis, ROS, mitochondrial function and TEM

TUNEL staining was performed using the DeadEnd™ Fluorometric TUNEL System (cat. no. G3250; Promega Corporation, Madison, WI, USA). Cells were fixed, permeabilized, incubated with the TUNEL reaction mixture, counterstained with propidium iodide, and imaged by fluorescence microscopy. Five random fields were analyzed per sample.

Apoptosis was also quantified using an Annexin V-FITC Apoptosis Detection Kit (cat. no. C1062M; Beyotime Biotechnology, Shanghai, China). After 48 h of treatment, cells were harvested, stained

according to the manufacturer's protocol, and analyzed using BD FACSCalibur (BD Biosciences, San Jose, CA, USA) equipped with a 488-nm laser. At least 10,000 events were collected for each sample.

Intracellular ROS was detected using a Reactive Oxygen Species Assay Kit (cat. no. S0033M; Beyotime Biotechnology, Shanghai, China). Treated cells were incubated with 10 μM DCFH-DA for 30 min at 37°C in the dark, and fluorescence was recorded at excitation/emission wavelengths of 488/525 nm. Mitochondrial membrane potential was assessed using a Mitochondrial Membrane Potential Assay Kit with JC-1 (cat. no. C2006; Beyotime Biotechnology, Shanghai, China). The red/green fluorescence ratio was used as an indicator of mitochondrial depolarization. For transmission electron microscopy, treated cells were fixed in 2.5% glutaraldehyde, processed through dehydration and embedding, sectioned, stained with uranyl acetate and lead citrate, and imaged using a JEM-1400 transmission electron microscope at 80 kV.

Western blotting

Western blotting
Cells were treated with vehicle, PTL, imatinib, or PTL plus imatinib for 48 h. Total protein was extracted using RIPA lysis buffer (cat. no. P0013C; Beyotime Biotechnology, Shanghai, China) supplemented with protease and phosphatase inhibitors. Protein concentrations were measured using a BCA Protein Assay Kit (cat. no. P0012; Beyotime Biotechnology, Shanghai, China). Equal amounts of protein (20 μg per lane) were separated by SDS-PAGE and transferred to PVDF membranes (MilliporeSigma, Burlington, MA, USA).

Membranes were blocked with 5% non-fat milk in TBST for 1 h at room temperature and then incubated overnight at 4°C with primary antibodies against cleaved-caspase-3, Bcl-2, Bax, IRE1α, phospho-IRE1α, CHOP, GRP78/BiP, LC3B/LC3-I/II, Beclin-1, PINK1, and GAPDH. Detailed antibody information, including manufacturers, catalog numbers, and dilutions, is provided in Supplementary Table S1. After washing, membranes were incubated with HRP-conjugated goat anti-rabbit IgG H&L (cat. no. ab6721; Abcam, Cambridge, UK) or HRP-conjugated goat anti-mouse IgG H&L (cat. no. ab6789; Abcam, Cambridge, UK). Bands were visualized using an ECL Substrate Kit (High Sensitivity) (cat. no. ab133406; Abcam, Cambridge, UK) and quantified with ImageJ. GAPDH was used as the loading control.

Public datasets and bioinformatics analysis

The public RNA-expression datasets GSE69465 and GSE155800 were downloaded from the NCBI Gene Expression Omnibus and used to examine transcriptional programs associated with imatinib response in GIST. Data preprocessing and normalization were performed according to the corresponding platform annotation files.

Differential expression analysis was performed in R (v4.3.3) using limma (v3.58.0). Genes with |log2 fold change| > 1 and adjusted $P < 0.05$ were considered differentially expressed. Functional enrichment

analysis was performed using clusterProfiler (v4.10.0) and org.Hs.eg.db (v3.18.0). Gene set enrichment analysis was performed using Hallmark gene sets from the Molecular Signatures Database and fgsea (v1.26.0). PCA plots, heatmaps, volcano plots, enrichment plots, and ROC curves were generated using ggplot2 (v3.5.0), enrichplot (v1.22.0), and pheatmap (v1.0.12), as appropriate.

Xenograft experiment and histology

Female BALB/c nude mice (cat. no. SM-014; Shanghai Model Organisms Center, Inc., Shanghai, China), aged 6 weeks and weighing 20–25 g, were housed under specific-pathogen-free conditions. GIST-T1 cells (1 × 10^7 cells in 100 μL PBS) were subcutaneously injected into the right axilla of each mouse. When tumor volume reached approximately 50 mm3, mice were randomly assigned to four groups (n = 5 per group): vehicle, PTL, imatinib, and PTL plus imatinib. Imatinib was administered by oral gavage at 25 mg/kg twice daily, and PTL was administered by intraperitoneal injection at 10 mg/kg every other day.

Tumor length and width were measured with calipers, and tumor volume was calculated as (length × width2)/2. Body weight was monitored throughout treatment. After approximately 4 weeks of treatment, mice were euthanized by CO2 inhalation according to institutional animal-care guidelines. Tumors were excised, photographed, weighed, and fixed in 10% neutral buffered formalin. Fixed tumor tissues were embedded in paraffin, sectioned at 4 μm, and stained with hematoxylin and eosin for histological analysis. The animal experiment was approved by the Laboratory Animal Ethics Committee of Yanbian University (approval no. YD20240311016).

Statistical analysis

Data are presented as mean ± SD unless otherwise indicated. Comparisons among multiple groups at a single time point were performed using one-way ANOVA followed by Tukey's multiple-comparisons test. Dunnett's test was used when comparisons were made only against the control group. Time-course data were analyzed using two-way ANOVA. If assumptions of normality or homogeneity of variance were not met, the Kruskal-Wallis test followed by Dunn's post hoc test was applied. A two-sided $P < 0.05$ was considered statistically significant.

Results

Transcriptomic analyses suggested stress- and cell-fate-related programs associated with imatinib response

The overall study workflow is summarized in Fig. 1a. Public GIST transcriptomic datasets were first analyzed to identify biological programs associated with imatinib response, and these findings were used to guide pharmacological validation in GIST-T1 and GIST-882 cells and in a GIST-T1 xenograft model. These analyses were used as hypothesis-generating resources rather than as independent proof of causality.

Principal component analysis showed transcriptional separation between imatinib-sensitive and imatinib-resistant samples in both GSE69465 and GSE155800, although the degree of separation differed between datasets (Fig. 1b, c). Heatmap visualization of selected differentially expressed genes further supported group-level transcriptional differences (Fig. 1d, e). Gene-set enrichment and pathway-summary analyses highlighted programs related to migration, cell-cycle regulation, oxidative stress, unfolded protein response, apoptosis, autophagy, mitochondrial regulation, epithelial–mesenchymal transition, inflammatory signaling, and survival-associated pathways (Fig. 1f–h). ROC analysis showed discriminatory performance of the selected transcriptomic signature, with an AUC of 0.880 (Fig. 1i). Together, these analyses supported the working hypothesis that imatinib response in GIST is associated with broader stress-handling and cell-fate regulatory programs.

PTL and imatinib inhibited GIST cell growth, and the combination enhanced functional suppression

Forty-eight-hour dose–response analysis showed concentration-dependent growth inhibition by PTL in both cell lines (Fig. 2a). GIST-T1 cells were more sensitive to PTL than GIST-882 cells, with estimated IC50 values of approximately 20 μM and 27 μM, respectively. Imatinib also produced dose-dependent inhibition, with estimated IC50 values of approximately 0.10 μM in GIST-T1 cells and 0.30 μM in GIST-882 cells (Fig. 2b). Complete time-course inhibition data are shown in ESM Fig. S1.

At the selected working concentrations, PTL and imatinib alone reduced malignant phenotypes, whereas PTL plus imatinib produced stronger suppression than either monotherapy. In wound-healing assays, the combination markedly reduced wound closure in both cell lines (Fig. 2c–f). Colony-formation assays showed a similar pattern, with the fewest colonies observed in the combination groups (Fig. 2g–i). These findings indicate that PTL enhances the growth- and migration-suppressive effects of imatinib in GIST cells.

PTL plus imatinib increased apoptotic cell death in GIST-T1 and GIST-882 cells

TUNEL staining showed an apparent increase in TUNEL-positive signals after PTL plus imatinib treatment compared with vehicle or single-agent treatment in both cell lines (Fig. 3a, b). Annexin V-FITC/PI flow cytometry further confirmed that total apoptotic fractions were highest in the combination groups (Fig. 3c–f). Although the absolute apoptotic response differed between GIST-T1 and GIST-882 cells, the direction of change was consistent.

Western blotting supported these apoptosis-related findings. Combination treatment reduced Bcl-2 expression and increased the Bax/Bcl-2 ratio in both cell lines (Fig. 3g–j). Cleaved-caspase-3-associated protein signals were also altered after treatment, with a cell-line-dependent densitometric pattern. Together, these data indicate that PTL potentiates imatinib-associated apoptotic cell death in GIST cells.

Combination treatment engaged stress-associated signaling and mitochondrial injury

In GIST-T1 cells, PTL plus imatinib increased GRP78/BiP, p-IRE1α/IRE1α, and CHOP compared with vehicle control and monotherapy groups (Fig. 4a, b). Similar ER-stress-associated changes were observed in GIST-882 cells, although the magnitude differed between cell lines (Fig. 4c, d). These findings suggest that ER-stress-associated signaling was engaged after combined treatment.

Autophagy- and mitochondrial-stress-associated markers were also affected. In GIST-T1 cells, PTL plus imatinib increased mitochondrial PINK1, LC3-II/LC3-I, and Beclin-1 (Fig. 4e, f). In GIST-882 cells, PINK1 and Beclin-1 also increased, whereas LC3-II/LC3-I showed a related but less pronounced pattern (Fig. 4g, h). Because autophagic flux was not directly measured, these results are interpreted as autophagy-associated marker changes rather than definitive evidence of increased autophagic flux.

JC-1 staining showed loss of mitochondrial membrane potential after combined treatment, as indicated by reduced red fluorescence and increased green fluorescence in both cell lines (Fig. 4i, j). Transmission electron microscopy revealed mitochondrial swelling and cristae disruption, particularly in the combination groups (Fig. 4k, m). Consistently, intracellular ROS levels were highest after PTL plus imatinib treatment (Fig. 4l, n). These results indicate that the enhanced apoptotic response was accompanied by ER-stress-associated signaling, ROS accumulation, autophagy-associated marker changes, and mitochondrial damage.

PTL enhanced imatinib activity in vivo

The antitumor effect of PTL plus imatinib was further evaluated in a GIST-T1 xenograft model. Body weight remained relatively stable in the control and PTL groups, whereas body-weight loss was most evident in the imatinib group (Fig. 5a). The combination group showed some body-weight reduction, but this decrease was less pronounced than that observed with imatinib monotherapy (Fig. 5a). These findings suggest that the combination did not produce greater body-weight loss than imatinib alone under the present dosing schedule.

Tumor-growth curves showed that the combination group had the slowest tumor growth among all groups (Fig. 5b). Representative images of excised tumors showed smaller tumors in the combination group than in the vehicle control or monotherapy groups (Fig. 5c). Endpoint tumor-weight analysis showed a stepwise decreasing trend, with the lowest tumor weights observed after PTL plus imatinib treatment (Fig. 5d). The reductions in the PTL and imatinib monotherapy groups did not reach statistical significance compared with control, whereas PTL plus imatinib significantly reduced tumor weight (Fig. 5d). H&E staining further showed more evident treatment-associated histological changes in the combination group (Fig. 5e). Together, these findings support an enhanced in vivo antitumor effect of PTL plus imatinib in the GIST-T1 xenograft model.

Discussion

This study supports PTL as a potential imatinib-sensitizing compound in GIST. Across two GIST cell lines, PTL plus imatinib produced stronger growth suppression than either monotherapy and increased apoptotic cell death. The combination was accompanied by ROS accumulation, mitochondrial injury, ER-stress-associated signaling, and altered autophagy-related markers (Fig. 2–4). Xenograft testing further showed a stronger antitumor effect with combined treatment than with either agent alone (Fig. 5). These findings position PTL as a candidate adjuvant that may enhance the pharmacological effect of imatinib.

This question is clinically relevant because imatinib remains first-line systemic therapy for advanced or unresectable GIST with imatinib-sensitive KIT or PDGFRA alterations [1, 2]. Despite its benefit, acquired resistance is common and may result from secondary kinase-domain mutations, tumor heterogeneity, survival pathway reactivation, and non-KIT/PDGFRA-dependent adaptive states [3, 4]. Later-line TKIs have improved outcomes in selected settings, as shown by ripretinib and avapritinib [5, 6]. However, sequential kinase inhibition does not fully solve disease persistence. This supports testing compounds that deepen imatinib response through complementary mechanisms.

The public datasets helped shape this rationale. In both GSE69465 and GSE155800, imatinib response was associated with differences in apoptosis-, stress-, survival-, inflammatory-, and EMT-related programs (Fig. 1). These data should not be overinterpreted because public datasets differ in platform, sample composition, and clinical annotation. Moreover, ER stress, mitochondrial injury, autophagy, and apoptosis are often regulated through phosphorylation, organelle damage, protein turnover, and flux rather than mRNA abundance alone [11, 12]. Still, the transcriptomic results provided useful biological context for testing PTL as a stress-modulating adjuvant.

The two cell lines showed different sensitivity profiles. GIST-T1 cells were more sensitive to both PTL and imatinib than GIST-882 cells, consistent with the biological heterogeneity of GIST models and tumors [1, 3, 4]. Notably, the combination retained enhanced activity in both cell lines. This strengthens the central observation that PTL can increase the biological effect of imatinib across more than one GIST context, although it does not imply that all GIST genotypes would respond similarly.

Apoptosis appeared to be a major outcome of combined treatment. TUNEL staining, Annexin V/PI analysis, and western blotting showed higher apoptotic activity in the PTL plus imatinib groups (Fig. 3). PTL has previously been described as a cooperating agent in anticancer treatment, with reported effects on NF-κB signaling, pro-survival pathways, and apoptosis [8]. Our data extend this concept to GIST models.

The ROS and mitochondrial findings provide a plausible link between PTL exposure and the enhanced apoptotic phenotype. PTL has been associated with oxidative stress, glutathione depletion, mitochondrial membrane-potential loss, and apoptosis in several cancer-cell contexts [10, 13]. PTL plus imatinib produced the strongest ROS signal, reduced mitochondrial membrane potential, and induced mitochondrial ultrastructural injury (Fig. 4i–n). These data support a ROS-associated mitochondrial stress response. However, because ROS-scavenger rescue was not performed, they should not be interpreted as definitive proof of ROS dependence.

ER-stress-associated signaling was also engaged by the combination. PTL plus imatinib increased p-IRE1α/IRE1α and CHOP in both cell lines (Fig. 4a–d). ER stress may support adaptation when the unfolded protein response restores proteostasis, but prolonged or severe ER stress can shift cells toward apoptosis [11, 12]. The data suggest a stress state associated with apoptotic commitment, although pathway rescue experiments are required to define causality.

Autophagy-related findings require caution. LC3-II/LC3-I and Beclin-1 changes indicate autophagy-associated marker alterations, but they cannot distinguish increased autophagosome formation from impaired lysosomal degradation. This distinction matters because autophagy can either protect cancer cells or contribute to cell death depending on context [14, 15]. In GIST, imatinib-induced autophagy has been reported as a survival mechanism, and autophagy inhibition can promote imatinib-associated GIST cell death [7, 16]. Therefore, these findings are best described as autophagy-associated changes accompanying the response.

PTL monotherapy produced only a modest, non-significant reduction in endpoint tumor weight. Imatinib also showed a decreasing trend but did not significantly reduce endpoint tumor weight versus control in the current dataset. Notably, PTL plus imatinib produced the lowest endpoint tumor weights and significantly reduced tumor weight compared with control (Fig. 5d). Body-weight monitoring suggested that the combination did not cause greater body-weight loss than imatinib alone (Fig. 5a) under the present dosing schedule, suggesting that PTL enhanced the in vivo antitumor effect of imatinib without an obvious additional body-weight burden.

Several limitations should be noted. First, the in vivo study used only GIST-T1 xenografts, and broader imatinib-resistant or mutation-defined models are needed. Second, the mechanistic data are based mainly on endpoint assays. ROS accumulation, mitochondrial injury, ER-stress-associated signaling, autophagy-associated marker changes, and apoptosis occurred together, but rescue experiments targeting ROS, ER stress, or autophagy were not performed. Third, formal drug-combination modeling was not performed, so the results should be interpreted as an enhanced combined effect rather than quantitative pharmacological synergy. Finally, body weight is a limited safety readout; organ histology, blood chemistry, pharmacokinetic/pharmacodynamic analysis, and formulation optimization will be required before PTL or PTL-derived compounds can be considered for further translational development.

Conclusion

This study provides preclinical evidence that PTL enhances the antitumor activity of imatinib in GIST models. In GIST-T1 and GIST-882 cells, PTL plus imatinib produced stronger inhibition of cell growth, migration, and colony formation than either monotherapy. The combination also increased apoptotic cell death and was accompanied by ROS accumulation, mitochondrial injury, ER-stress-associated signaling, and autophagy-associated marker changes. In the GIST-T1 xenograft model, PTL plus imatinib produced the lowest endpoint tumor weights and significantly reduced tumor weight compared with control, without greater body-weight loss than imatinib alone under the present dosing schedule. These results

support PTL as a potential adjuvant candidate for improving imatinib response in GIST, but further studies are needed to define causality, safety, pharmacokinetics, formulation optimization, and efficacy in broader imatinib-resistant or mutation-defined models.

Declarations

Competing interests

The authors have no relevant financial or non-financial interests to disclose.

Ethics approval

The animal experiment was approved by the Laboratory Animal Ethics Committee of Yanbian University (approval no. YD20240311016). All procedures were performed in accordance with the Yanbian University Laboratory Animal Management Rules.

Consent to participate

Not applicable.

Consent for publication

Not applicable.

Funding

This work was supported by the Natural Science Research Foundation of Jilin Province for Sciences and Technology (YDZJ202201ZYTS227, Toufeng Jin); by the Postdoctoral Researcher Talent Selection and Funding Program of Jilin Province (012025297, Chuang-Ming Zheng). The funders had no role in study design, data collection and analysis, decision to publish, or preparation of the manuscript.

Author Contribution

L.P. contributed to conceptualization, methodology, investigation, data curation, formal analysis, visualization, software, validation, writing – original draft, and writing – review and editing. Z.P. contributed to methodology, investigation, validation, data curation, and writing – review and editing. C.-H.Z. contributed to resources, project administration, and writing – review and editing. D.X. contributed to conceptualization, methodology, investigation, data curation, formal analysis, and writing – review and editing. X.-H.L. contributed to investigation, methodology, and visualization. P.W. contributed to resources, methodology, data curation, formal analysis, visualization, software, and validation. C.P.

contributed to data curation, software, and validation. C.-M.Z. contributed to conceptualization, supervision, project administration, funding acquisition, and writing – review and editing. T.J. contributed to conceptualization, supervision, funding acquisition, resources, and writing – review and editing. All authors read and approved the final manuscript.

Data Availability

The public datasets analyzed in this study are available from the NCBI Gene Expression Omnibus under accession numbers GSE69465 and GSE155800. The remaining data supporting the findings of this study are available from the corresponding author upon reasonable request.

References

1. Serrano C, Martín-Broto J, Asencio-Pascual JM et al (2023) 2023 GEIS Guidelines for gastrointestinal stromal tumors. Ther Adv Med Oncol 15:17588359231192388. https://doi.org/10.1177/17588359231192388
2. Demetri GD, von Mehren M, Blanke CD et al (2002) Efficacy and safety of imatinib mesylate in advanced gastrointestinal stromal tumors. N Engl J Med 347(7):472–480. https://doi.org/10.1056/NEJMoa020461
3. Serrano C, Mariño-Enríquez A, Tao DL et al (2019) Complementary activity of tyrosine kinase inhibitors against secondary kit mutations in imatinib-resistant gastrointestinal stromal tumours. Br J Cancer 120(6):612–620. https://doi.org/10.1038/s41416-019-0389-6
4. He C, Wang Z, Yu J et al (2024) Current Drug Resistance Mechanisms and Treatment Options in Gastrointestinal Stromal Tumors: Summary and Update. Curr Treat Options Oncol 25(11):1390–1405. https://doi.org/10.1007/s11864-024-01272-7
5. Blay JY, Serrano C, Heinrich MC et al (2020) Ripretinib in patients with advanced gastrointestinal stromal tumours (INVICTUS): a double-blind, randomised, placebo-controlled, phase 3 trial. Lancet Oncol 21(7):923–934. https://doi.org/10.1016/S1470-2045(20)30168-6
6. Heinrich MC, Jones RL, von Mehren M et al (2020) Avapritinib in advanced PDGFRA D842V-mutant gastrointestinal stromal tumour (NAVIGATOR): a multicentre, open-label, phase 1 trial. Lancet Oncol 21(7):935–946. https://doi.org/10.1016/S1470-2045(20)30269-2
7. Gupta A, Roy S, Lazar AJF et al (2010) Autophagy inhibition and antimalarials promote cell death in gastrointestinal stromal tumor (GIST). Proc Natl Acad Sci U S A 107(32):14333–14338. https://doi.org/10.1073/pnas.1000248107
8. Sztiller-Sikorska M, Czyz M (2020) Parthenolide as Cooperating Agent for Anti-Cancer Treatment of Various Malignancies. Pharmaceuticals 13(8):194. https://doi.org/10.3390/ph13080194
9. An T, Yin H, Lu Y et al (2022) The Emerging Potential of Parthenolide Nanoformulations in Tumor Therapy. Drug Des Devel Ther 16:1255–1272. https://doi.org/10.2147/DDDT.S355059

10. Jorge J, Neves J, Alves R et al (2023) Parthenolide Induces ROS-Mediated Apoptosis in Lymphoid Malignancies. Int J Mol Sci 24(11):9167. https://doi.org/10.3390/ijms24119167
11. Fu X, Cui J, Meng X et al (2021) Endoplasmic reticulum stress, cell death and tumor: Association between endoplasmic reticulum stress and the apoptosis pathway in tumors (Review). Oncol Rep 45(3):801–808. https://doi.org/10.3892/or.2021.7933
12. Zhang W, Shi Y, Oyang L et al (2024) Endoplasmic reticulum stress-a key guardian in cancer. Cell Death Discov 10(1):343. https://doi.org/10.1038/s41420-024-02110-3
13. Han D, Zhu W, Chen Y et al (2024) Parthenolide induces ROS-dependent cell death in human gastric cancer cell. Adv Clin Exp Med Off Organ Wroclaw Med Univ 33(11):1237–1245. https://doi.org/10.17219/acem/175152
14. Ye J, Zhang J, Zhu Y et al (2023) Targeting autophagy and beyond: Deconvoluting the complexity of Beclin-1 from biological function to cancer therapy. Acta Pharm Sin B 13(12):4688–4714. https://doi.org/10.1016/j.apsb.2023.08.008
15. Cao Z, Tian K, Ran Y et al (2024) Beclin-1: a therapeutic target at the intersection of autophagy, immunotherapy, and cancer treatment. Front Immunol 15:1506426. https://doi.org/10.3389/fimmu.2024.1506426
16. Zheng S, Shu Y, Lu Y et al (2020) Chloroquine Combined with Imatinib Overcomes Imatinib Resistance in Gastrointestinal Stromal Tumors by Inhibiting Autophagy via the MAPK/ERK Pathway. OncoTargets Ther 13:6433–6441. https://doi.org/10.2147/OTT.S256935

Figures

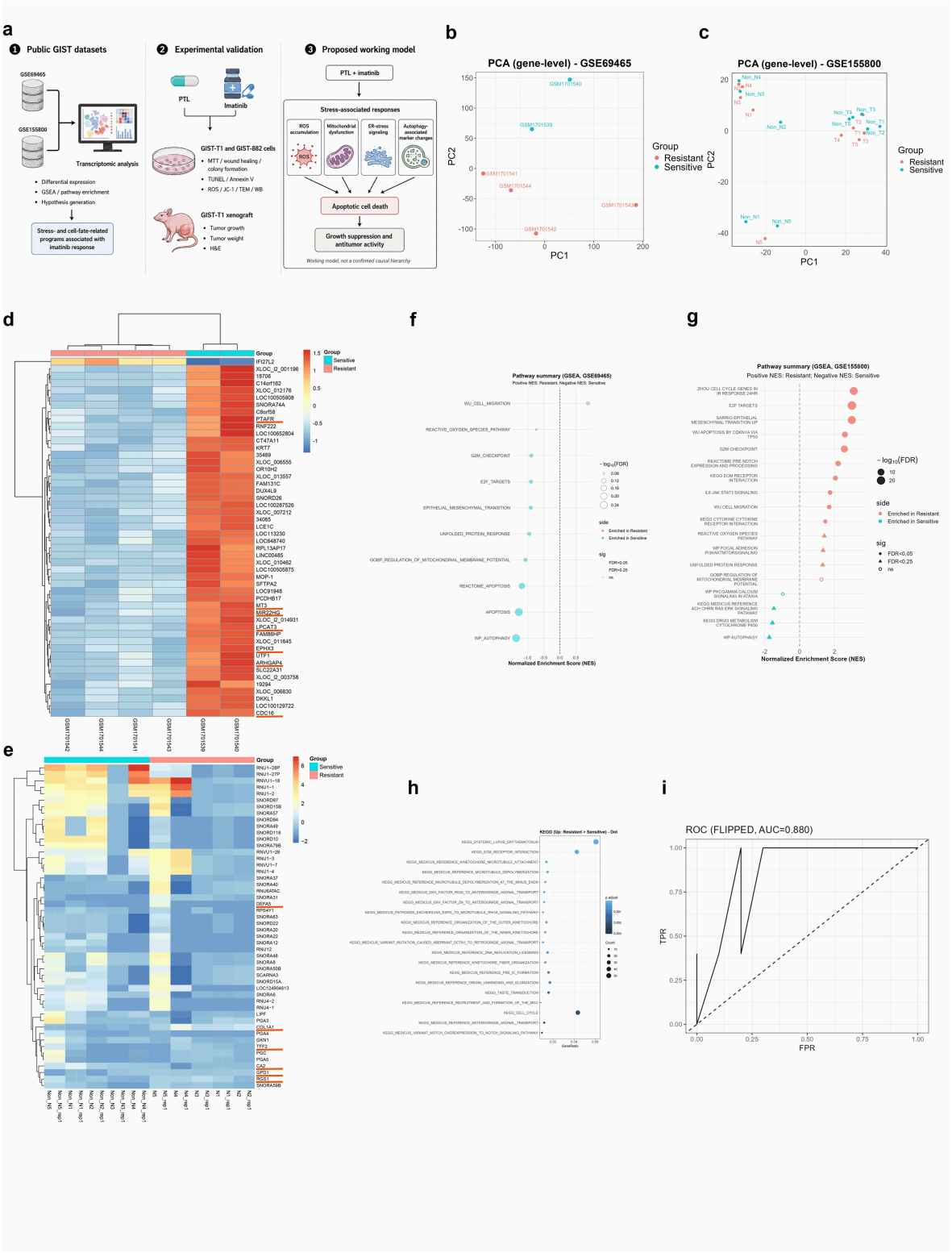


Figure 1

Study workflow and transcriptomic rationale for testing PTL as an imatinib-sensitizing compound in GIST.

a Schematic workflow summarizing public transcriptomic analysis, experimental validation in GIST-T1 and GIST-882 cells, in vivo validation in a GIST-T1 xenograft model, and the proposed working model.

Public GIST datasets were analyzed to identify biological programs associated with imatinib response, followed by pharmacological testing of PTL, imatinib, and PTL plus imatinib. b Principal component analysis of GSE69465 showing transcriptional differences between imatinib-sensitive and imatinib-resistant GIST samples. c Principal component analysis of GSE155800 showing group-level transcriptional differences between imatinib-sensitive and imatinib-resistant samples. d Heatmap visualization of selected differentially expressed genes in GSE69465. e Heatmap visualization of selected differentially expressed genes in GSE155800. f Gene-set enrichment summary of GSE69465 showing selected pathways related to migration, oxidative stress, cell-cycle regulation, unfolded protein response, apoptosis, autophagy, mitochondrial regulation, and epithelial–mesenchymal transition. g Gene-set enrichment summary of GSE155800 showing selected pathways associated with cell-cycle regulation, inflammatory signaling, apoptosis, oxidative stress, unfolded protein response, autophagy, mitochondrial regulation, and survival-associated programs. h KEGG enrichment analysis of genes upregulated in resistant versus sensitive samples in GSE155800. i ROC analysis of the selected transcriptomic signature. Public transcriptomic datasets were used as hypothesis-generating resources rather than independent proof of mechanism.

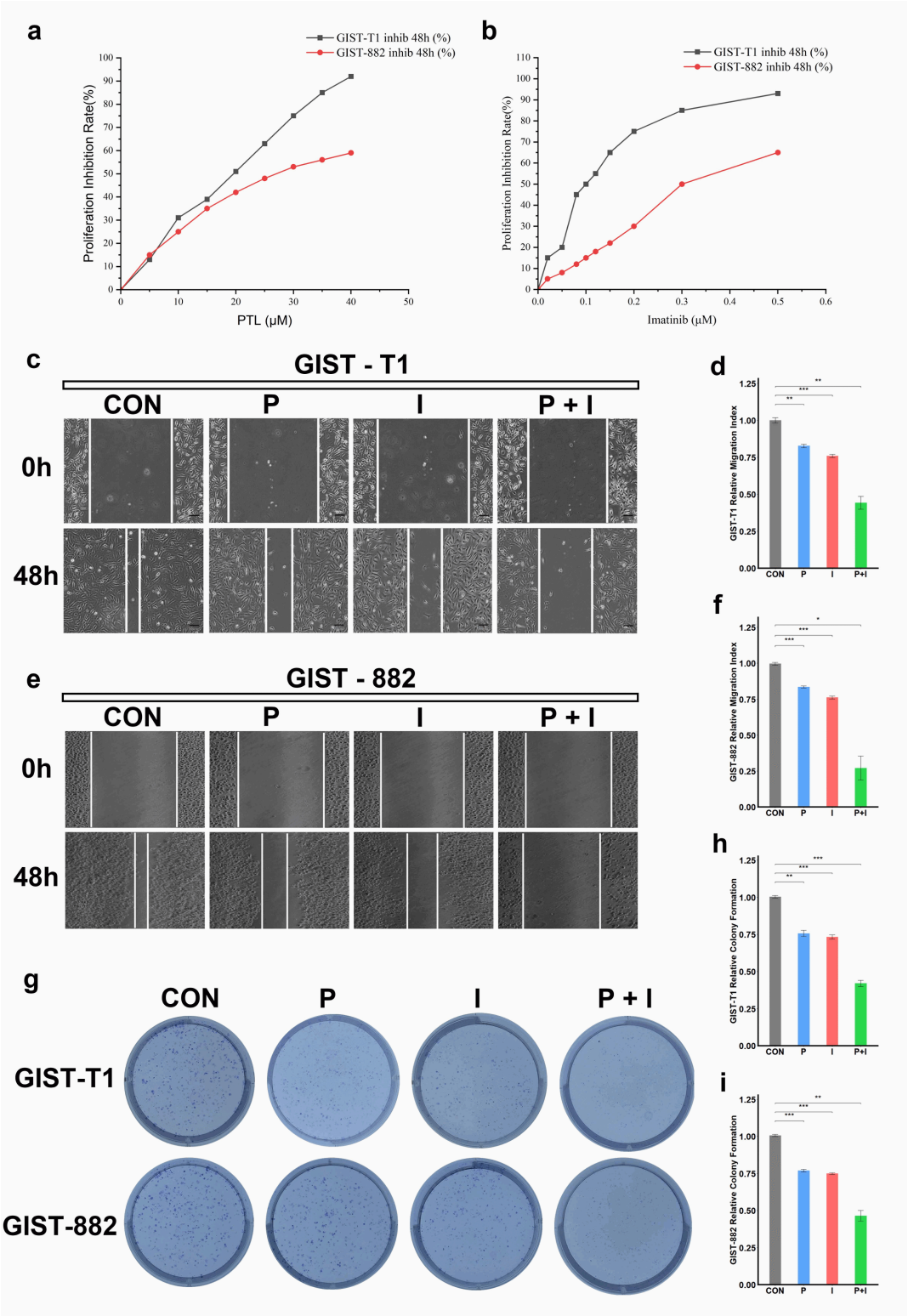


Figure 2

PTL enhances the growth- and migration-suppressive effects of imatinib in GIST cells.

a Forty-eight-hour dose–response inhibition curves for PTL in GIST-T1 and GIST-882 cells. b Forty-eight-hour dose–response inhibition curves for imatinib in GIST-T1 and GIST-882 cells. c Representative wound-healing images of GIST-T1 cells treated with vehicle control, PTL, imatinib, or PTL plus imatinib

for 48 h. d Quantification of the relative migration index in GIST-T1 cells. e Representative wound-healing images of GIST-882 cells treated with vehicle control, PTL, imatinib, or PTL plus imatinib for 48 h. f Quantification of the relative migration index in GIST-882 cells. g Representative colony-formation images of GIST-T1 and GIST-882 cells after treatment with vehicle control, PTL, imatinib, or PTL plus imatinib. h Quantification of relative colony formation in GIST-T1 cells. i Quantification of relative colony formation in GIST-882 cells. CON, vehicle control; P, PTL; I, imatinib; P+I, PTL plus imatinib. Data are shown as mean ± SD from independent biological replicates. *P < 0.05, **P < 0.01, ***P < 0.001.

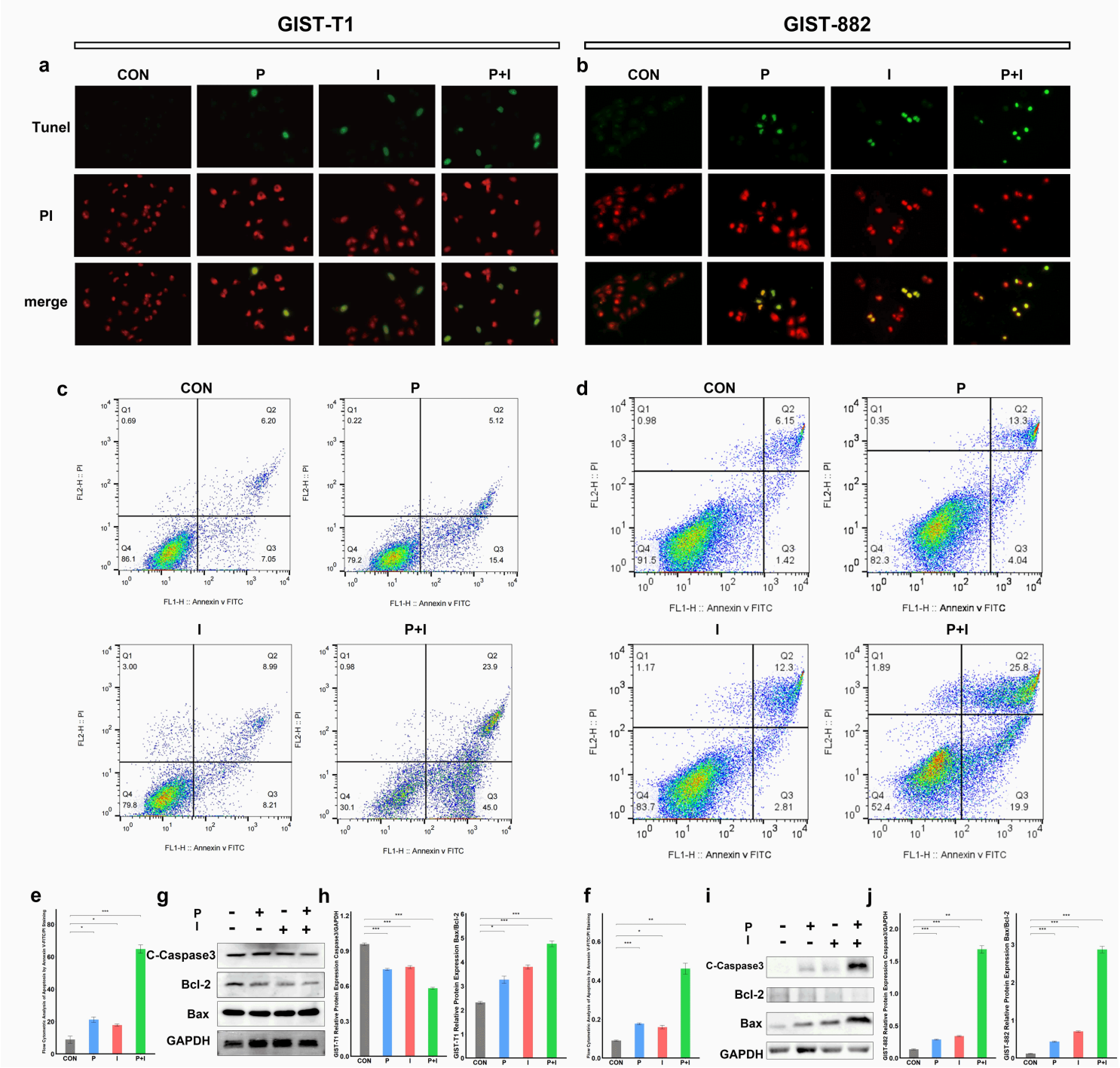


Figure 3

PTL plus imatinib increases apoptotic cell death in GIST-T1 and GIST-882 cells.

a Representative TUNEL staining images of GIST-T1 cells treated with vehicle control, PTL, imatinib, or PTL plus imatinib. b Representative TUNEL staining images of GIST-882 cells after the indicated treatments. Green fluorescence indicates TUNEL-positive cells, red fluorescence indicates PI-stained nuclei, and merged images are shown. c Representative Annexin V-FITC/PI flow-cytometry plots of GIST-T1 cells. d Representative Annexin V-FITC/PI flow-cytometry plots of GIST-882 cells. e Quantification of total apoptotic cells in GIST-T1 cells, calculated as the sum of early and late apoptotic fractions. f Quantification of total apoptotic cells in GIST-882 cells. g Representative western blots of cleaved-caspase-3, Bcl-2, Bax, and GAPDH in GIST-T1 cells. h Densitometric quantification of cleaved-caspase-3/GAPDH and Bax/Bcl-2 ratio in GIST-T1 cells. i Representative western blots of cleaved-caspase-3, Bcl-2, Bax, and GAPDH in GIST-882 cells. j Densitometric quantification of cleaved-caspase-3/GAPDH and Bax/Bcl-2 ratio in GIST-882 cells. CON, vehicle control; P, PTL; I, imatinib; P+I, PTL plus imatinib. Data are shown as mean ± SD. *P < 0.05, **P < 0.01, ***P < 0.001. Original uncropped blot images are provided in ESM Fig. S3.

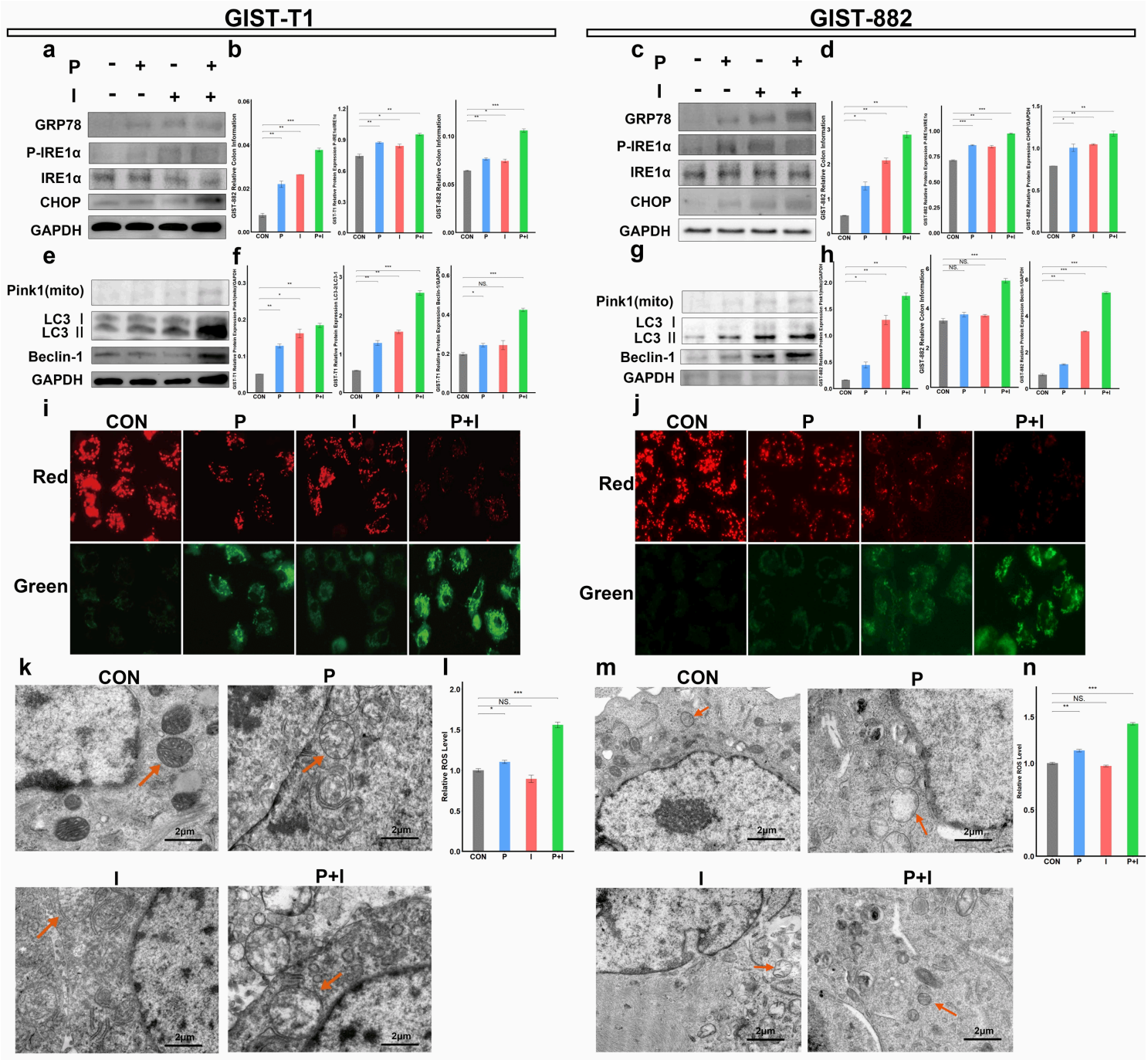


Figure 4

PTL plus imatinib engages ER-stress-associated signaling, autophagy-associated marker changes, ROS accumulation, and mitochondrial injury in GIST cells.

a Representative western blots of GRP78/BiP, p-IRE1α, IRE1α, CHOP, and GAPDH in GIST-T1 cells. b Densitometric quantification of GRP78/GAPDH, p-IRE1α/IRE1α, and CHOP/GAPDH in GIST-T1 cells. c Representative western blots of GRP78/BiP, p-IRE1α, IRE1α, CHOP, and GAPDH in GIST-882 cells. d Densitometric quantification of GRP78/GAPDH, p-IRE1α/IRE1α, and CHOP/GAPDH in GIST-882 cells. e Representative western blots of mitochondrial PINK1, LC3-I/II, Beclin-1, and GAPDH in GIST-T1 cells. f Densitometric quantification of mitochondrial PINK1/GAPDH, LC3-II/LC3-I, and Beclin-1/GAPDH in GIST-

T1 cells. g Representative western blots of mitochondrial PINK1, LC3-I/II, Beclin-1, and GAPDH in GIST-882 cells. h Densitometric quantification of mitochondrial PINK1/GAPDH, LC3-II/LC3-I, and Beclin-1/GAPDH in GIST-882 cells. i Representative JC-1 staining images of GIST-T1 cells. Red fluorescence indicates mitochondrial aggregates, whereas green fluorescence indicates JC-1 monomers. j Representative JC-1 staining images of GIST-882 cells. k Representative transmission electron microscopy images of GIST-T1 cells showing mitochondrial ultrastructural changes. l Quantification of relative intracellular ROS levels in GIST-T1 cells. m Representative transmission electron microscopy images of GIST-882 cells showing mitochondrial ultrastructural changes. n Quantification of relative intracellular ROS levels in GIST-882 cells. CON, vehicle control; P, PTL; I, imatinib; P+I, PTL plus imatinib. Data are shown as mean ± SD. NS, not significant; *P < 0.05, **P < 0.01, ***P < 0.001. Original uncropped blot images are provided in ESM Figs. S4 and S5.

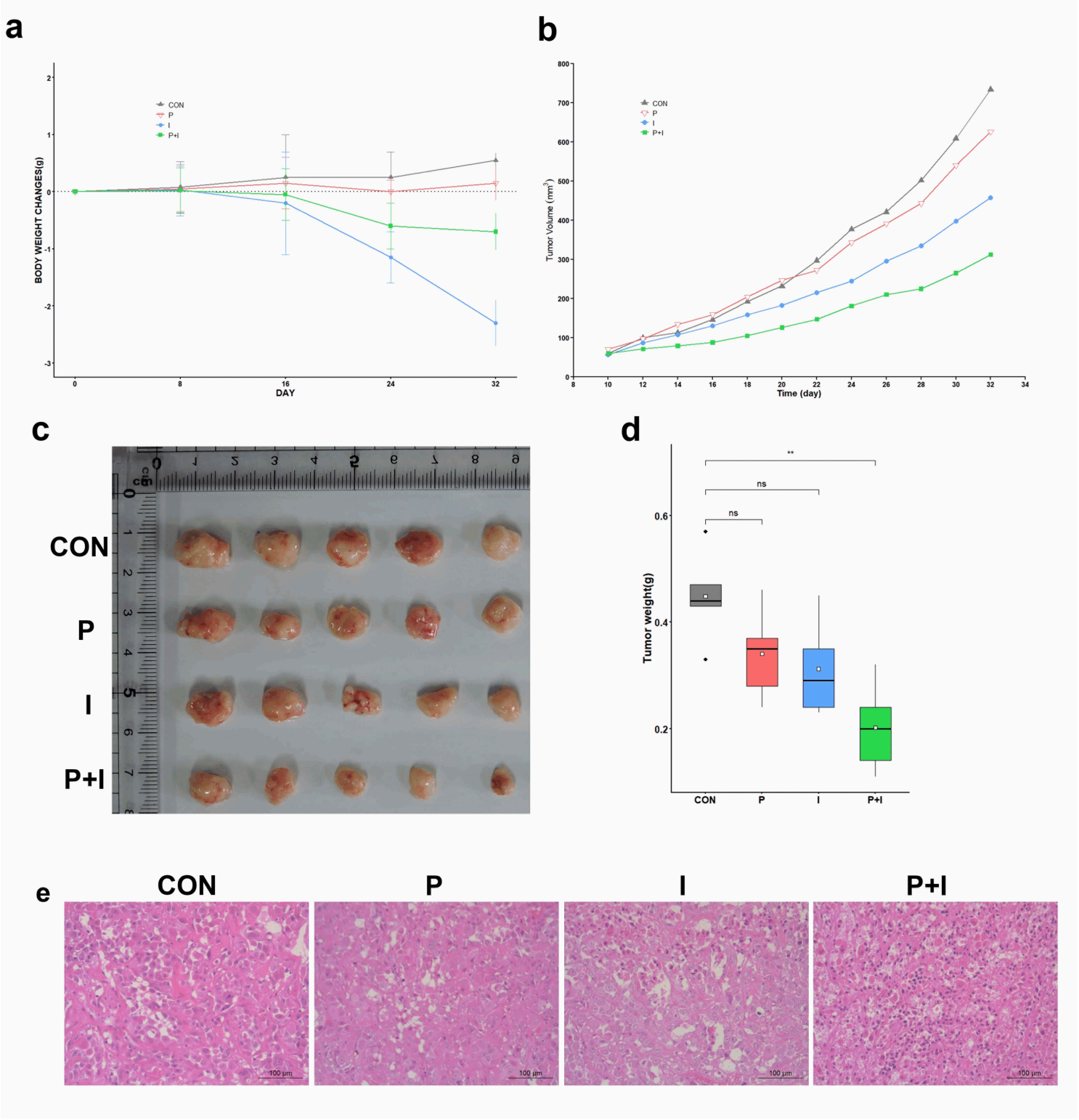


Figure 5

Xenograft validation of the antitumor effect of PTL plus imatinib.

a Body-weight changes during treatment. b Tumor-growth curves. c Representative images of excised xenograft tumors from the vehicle control, PTL, imatinib, and PTL plus imatinib groups. d Endpoint tumor weight. e Representative H&E staining of xenograft tumor tissues. GIST-T1 cells were subcutaneously

injected into the right axillary region of female BALB/c nude mice. When tumor volume reached approximately 50 mm³, mice were treated with vehicle control, PTL, imatinib, or PTL plus imatinib. Imatinib was administered by oral gavage at 25 mg/kg twice daily, and PTL was administered by intraperitoneal injection at 10 mg/kg every other day. Body-weight data are shown as mean ± SD. Tumor-weight data are shown as box plots. n = 5 per group. ns, not significant; **P < 0.01.

Supplementary Files

This is a list of supplementary files associated with this preprint. Click to download.

- ESM1.tif
- ESM2.tif
- ESM3.tif
- ESM4.tif
- ESM5.tif
- ESM6.xlsx